THE HARD X-RAY LUMINOSITY FUNCTION OF INTEGRAL DETECTED AGN

V. Beckmann[1], **C. R. Shrader**[1], **N. Gehrels**[1], **S. Soldi**[2], **and N. Produit**[2]

[1]*NASA Goddard Space Flight Center, Astrophysics Science Division, Code 661, Greenbelt, MD 20771, USA*
[2]*INTEGRAL Science Data Centre, Chemin d' Écogia 16, 1290 Versoix, Switzerland*

ABSTRACT

We have compiled a complete extragalactic sample based on $\sim 25,000\,\mathrm{deg}^2$ to a limiting flux of $3 \times 10^{-11}\,\mathrm{ergs\,cm^{-2}\,s^{-1}}$ ($\sim 7,000\,\mathrm{deg}^2$ to a flux limit of $10^{-11}\,\mathrm{ergs\,cm^{-2}\,s^{-1}}$) in the 20 – 40 keV band with *INTEGRAL*. We have constructed a detailed exposure map to compensate for effects of non-uniform exposure. The flux-number relation is best described by a power-law with a slope of $\alpha = 1.66 \pm 0.11$. The integration of the cumulative flux per unit area leads to $f_{20-40\,\mathrm{keV}} = 2.6 \times 10^{-10}\,\mathrm{ergs\,cm^{-2}\,s^{-1}\,sr^{-1}}$, which is about 1% of the known $20 - 40\,\mathrm{keV}$ X-ray background. We present the first luminosity function of AGN in the 20–40 keV energy range, based on 38 extragalactic objects detected by the imager IBIS/ISGRI on-board *INTEGRAL*. The luminosity function shows a smoothly connected two power-law form, with an index of $\gamma_1 = 0.8$ below, and $\gamma_2 = 2.1$ above the turn-over luminosity of $L_* = 2.4 \times 10^{43}\,\mathrm{ergs\,s^{-1}}$. The emissivity of all *INTEGRAL* AGN per unit volume is $W_{20-40\,\mathrm{keV}}(> 10^{41}\,\mathrm{ergs\,s^{-1}}) = 2.8 \times 10^{38}\,\mathrm{ergs\,s^{-1}\,h_{70}^3\,Mpc^{-3}}$. These results are consistent with those derived in the $2 - 20\,\mathrm{keV}$ energy band and do not show a significant contribution by Compton-thick objects. Because the sample used in this study is truly local ($\bar{z} = 0.022$), only limited conclusions can be drawn for the evolution of AGN in this energy band. But the objects explaining the peak in the cosmic X-ray background are likely to be either low luminosity AGN ($L_X < 10^{41}\,\mathrm{ergs\,s^{-1}}$) or of other type, such as intermediate mass black holes, clusters, and star forming regions, or they have to be at higher redshift.

Key words: galaxies: active; X-rays: galaxies; surveys; galaxies: Seyfert.

1. INTRODUCTION

The Galactic X-ray sky is dominated by accreting binary systems, while the extragalactic sky shows mainly active galactic nuclei (AGN) and clusters of galaxies. Studying the population of sources in X-ray bands has been a challenge ever since the first observations by rocket borne X-ray detectors [12]. At soft X-rays (0.1 – 2.4 keV) deep exposures by *ROSAT* have revealed an extragalactic population of mainly broad line AGN, such as type Seyfert 1 and quasars [14, 27]. In the 2 - 10 keV range surveys have been carried out with *ASCA* (e.g. Ueda et al. 2001), *XMM-Newton* (e.g. Hasinger 2004), and *Chandra* (e.g. Brandt et al. 2001) and have shown that the dominant extragalactic sources are more strongly absorbed than those within the *ROSAT* energy band. For a summary on the deep X-ray surveys below 10 keV see Brandt & Hasinger (2005). At higher energies the data become more scarce. Between a few keV and $\sim 1\,\mathrm{MeV}$, no all-sky survey using imaging instruments has been performed to date. The *Rossi X-ray Timing Explorer* (*RXTE*) sky survey in the $3 - 20\,\mathrm{keV}$ energy band revealed about 100 AGN, showing an even higher fraction of absorbed ($N_H > 10^{22}\,\mathrm{cm^{-2}}$) sources of about 60% [25]. *INTEGRAL* offers an unprecedented $> 20\,\mathrm{keV}$ collecting area and state-of-the-art detector electronics and background rejection capabilities. Notably, the imager IBIS enables us now to study a large portion of the sky. A first catalogue of AGN showed a similar fraction of absorbed objects as the *RXTE* survey [2]. The Burst Alert Telescope (BAT) of the *Swift* mission [11] operates in the 15 – 200 keV band and uses a detector similar to IBIS/ISGRI, but provides a field of view about twice the size. The BAT data of the first three months of the mission provided a high galactic latitute survey, including 44 AGN [20]. Within this sample a weak anti-correlation of luminosity versus intrinsic absorption was found as previously found in the $2 - 10\,\mathrm{keV}$ band [31, 17], revealing that most of the objects with luminosities $L_X > 3 \times 10^{43}\,\mathrm{ergs\,s^{-1}}$ show no intrinsic absorption. Markwardt et al. (2005) also pointed out that this luminosity corresponds to the break in the luminosity function.

Related to the compilation of AGN surveys in the hard X-rays is the question of what sources form the cosmic X-ray background (CXB). While the CXB below 20 keV has been the focus of many studies, the most reliable measurement in the 10 - 500 keV has been provided by the *High Energy Astronomical Observatory* (*HEAO 1*), launched in 1977 [21]. The most precise measurement provided by the UCSD/MIT Hard X-ray and Gamma-Ray instrument (*HEAO 1* A-4) shows that the CXB peaks at an energy of about $30\,\mathrm{keV}$ [21, 13]. The isotropic nature of the X-ray background points to an extragalactic origin, and as the brightest persistent sources are AGN, it was suggested early on that those objects are the main

source of the CXB (e.g. Setti & Woltjer 1989). In the soft X-rays this concept has been proven to be correct through the observations of the *ROSAT* deep X-ray surveys, which showed that 90% of the $0.5 - 2.0\,\mathrm{keV}$ CXB can be resolved into AGN [27]. At higher energies ($2 - 10\,\mathrm{keV}$), *ASCA* and *Chandra* surveys measured the hard X-ray luminosity function (XLF) of AGN and its cosmological evolution. These studies show that in this energy range the CXB can be explained by AGN, but with a higher fraction of absorbed ($N_H > 10^{22}\,\mathrm{cm}^{-2}$) objects than in the soft X-rays (e.g. Ueda et al. 2003). A study based on the *RXTE* survey by Sazonov & Revnivtsev (2004) derived the local hard X-ray luminosity function of AGN in the 3–20 keV band. They showed that the summed emissivity of AGN in this energy range is smaller than the total X-ray volume emissivity in the local Universe, and suggested that a comparable X-ray flux may be produced together by lower luminosity AGN, non-active galaxies and clusters of galaxies. Using the *HEAO 1*-A2 AGN, Shinozaki et al. (2006), however, obtained a local AGN emissivity which is about twice larger than the value of Sazonov & Revnivtsev (2004) but consistent with the estimates by Miyaji et al. (1994) which was based on the cross-correlation of the *HEAO 1*-A2 map with *IRAS* galaxies.

With the on-going observations of the sky by *INTEGRAL*, a sufficient amount of data is now available to derive the AGN hard X-ray luminosity function. In this paper we present analysis of recent observations performed by the *INTEGRAL* satellite, and compare the results with previous studies. In Section 2 we describe the AGN sample and in Section 3 the methods to derive the number-flux distribution of *INTEGRAL* AGN are presented together with the analysis of their distribution. Section 4 shows the local luminosity function of AGN as derived from our data, followed by a discussion of the results in Section 5. Throughout this work we applied a cosmology with $H_0 = 70\,\mathrm{km\,s^{-1}\,Mpc^{-1}}$ ($h_{70} = 1$), $k = 0$ (flat Universe), $\Omega_{matter} = 0.3$, and $\Lambda_0 = 0.7$, although a $\Lambda_0 = 0$ and $q_0 = 0.5$ cosmology does not change the results significantly because of the low redshifts in our sample.

2. THE *INTEGRAL* AGN SAMPLE

Observations in the X-ray to soft gamma-ray domain have been performed by the soft gamma-ray imager (20–1000 keV) ISGRI [18] on-board *INTEGRAL*.

The data used here are taken from orbit revolutions 19 - 137 and revolutions 142 - 149. The list of sources was derived from the analysis as described in Beckmann et al. (2006a,2006c). The analysis was performed using the Offline Science Analysis (OSA) software version 5.0 distributed by the ISDC (Courvoisier et al. 2003). Additional observations performed later led to further source detections within the survey area. We extracted spectra at those positions from the data following the same procedure. It is understood that most of those objects did not result in a significant detection $\geq 3\sigma$ in the data set used here, but it ensures completeness of the sample at a significance limit of 5σ (see Section 3).

The list of 73 sources has been reported in Beckmann et al. (2006c). 22 of the sources have Galactic latitudes $-10^\circ < b < +10^\circ$ (14, if we only consider the sources with significance $\geq 5\sigma$). In addition to the sample presented here, 8 new *INTEGRAL* sources with no identification have been detected in our survey with a significance of $\geq 5\sigma$. These un-identified sources, most of them in the Galactic Plane, are not included in this work. The significances used have been derived from the intensity maps produced by the OSA software. Fluxes are determined by integrating the best-fit spectral model over the 20–40 keV bandpass. The uncertainty in the absolute flux calibration is about 5%. The extracted images and source results are available in electronic form[1].

3. NUMBER-FLUX DISTRIBUTION OF *INTEGRAL* AGN

3.1. Completeness of the Sample

In order to compute the AGN number-flux relation it is necessary to have a complete and unbiased sample. Towards this end, one must understand the characteristics of the survey, such as the sky coverage and completeness for each subset of the total sample. Because of the in-homogeneous nature of the survey exposure map, we applied a significance limit rather than a flux limit to define a complete sample. The task is to find a significance limit which ensures that all objects above a given flux limit have been included. To test for completeness, the V_e/V_a-statistic has been applied, where V_e stands for the volume that is enclosed by the object, and V_a is the accessible volume, in which the object could have been found (Avni & Bahcall 1980).

In the case of no evolution $\langle V_e/V_a \rangle = 0.5$ is expected. This evolutionary test is applicable only to samples complete to a well-defined significance limit. It can therefore also be used to test the completeness of a sample. We performed a series of V_e/V_a-tests to the *INTEGRAL* AGN sample, assuming completeness limits in the range of 0.5σ up to 16σ ISGRI 20 – 40 keV significance. For a significance limit below the true completeness limit of the sample one expects the V_e/V_a-tests to derive a value $\langle V_e/V_a \rangle < \langle V_e/V_a \rangle_{true}$, where $\langle V_e/V_a \rangle_{true}$ is the true test result for a complete sample. Above the completeness limit the $\langle V_e/V_a \rangle$ values should be distributed around $\langle V_e/V_a \rangle_{true}$ within the statistical uncertainties. It appears that the sample becomes complete at a significance cutoff of approximately 5σ, which includes 38 AGN. The average value is $\langle V_e/V_a \rangle = 0.43 \pm 0.05$. This is consistent with the expected value of 0.5 at the 1.5σ level, suggesting no evolution and a uniform distribution in the local universe. It is unlikely that cosmological effects have an influence on the result, as the average red-

[1] http://heasarc.gsfc.nasa.gov/docs/integral/spi/pages/agn.html

shift in the sample is $\bar{z} = 0.022$, with a maximum redshift of $z = 0.13$. A positive cosmological evolution would result in a slightly higher value than 0.5. We would like to remind that we use the $\langle V_e/V_a \rangle$ test not to determine any cosmological effects, but use it to see at what significance level it returns a stable value.

3.2. Deriving the Area Corrected Number-Flux Distribution

A correct representation of the number flux distribution (i.e. $\log N_{>S}$ versus $\log S$, see Beckmann et al. 2006b) for the sample presented here must account for different exposure times comprising our survey, and the resulting sensitivity variations. We determine here the number density and thus the number of AGN above a given flux has to be counted and divided by the sky area in which they are detectable throughout the survey. We therefore first determined the exposure time in $64,620$ sky elements of $\sim 0.63\,\mathrm{deg}^2$ size within our survey. In each sky bin, the exposure is the sum of each individual exposure multiplied by the fraction of the coded field of view in this particular direction. The dead time and the good time intervals (GTI) are not taken into account but the dead time is fairly constant (around 20%) and GTI gaps are very rare in IBIS/ISGRI data. We excluded those fields with an exposure time less than 2 ks, resulting in $47,868$ sky elements with a total coverage of $9.89\,\mathrm{sr}$. The flux limit for a given significance limit should be a function of the square root of the exposure time, if no systematic effects apply, but this assumption cannot be made here. The nature of coded-mask imaging leads to accumulated systematic effects at longer exposure times. In order to achieve a correlation between the exposure time and the flux limit, we therefore used an empirical approach. For each object we computed what we will call its 5σ equivalent flux $f_{5\sigma}$, based on its actual flux f_X and its significance s: $f_{5\sigma} = f_X * 5/s$. We found a correlation between these $f_{5\sigma}$ values and exposure times, which has a scatter of $\lesssim 0.2\,\mathrm{dex}$. The correlation was then fitted by a smooth polynomial of third degree. This function was then used to estimate the limiting flux of each individual survey field. It must be noted that the individual limits are not important, but only the distribution of those flux limits.

Based on the flux limits for all survey fields, we are now able to construct the number flux distribution for the *INTEGRAL* AGN, determining for each source flux the total area in which the source is detectable with a 5σ detection significance in the $20 - 40\,\mathrm{keV}$ energy band. The resulting correlation is shown in Figure 1. The errors on the data points indicate 1σ uncertainties in the flux of the objects and the Poissonian errors for the number of objects per steradian.

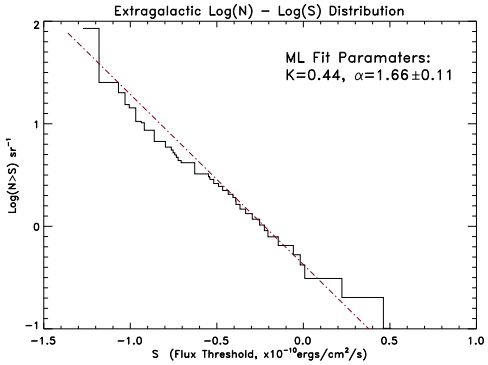

Figure 1. Number flux distribution per steradian of INTEGRAL AGN with a detection significance $> 5\sigma$. Blazars have been excluded. The maximum likelihood slope as described in Section 3.3 is 1.66 ± 0.11.

3.3. The Slope of the Number-Flux Distribution

We applied a maximum-likelihood (ML) algorithm to our empirical number-flux distribution to obtain a power-law approximation of the form $N(>S) = K \cdot S^{-\alpha}$. We note that we are fitting the "integrated" $N(>S)$ function, as distinct from the "differential" number-flux function. The latter entails binning the data, and thus some loss of information is incurred. The advantage of fitting the differential distribution is that a simple least squares procedure may be employed. However, given the modest size of our sample, the expected loss of accuracy was considered unacceptable.

For this analysis, we used the complete sub-sample of 38 sources for which the statistical significance of our flux determinations was at a level of 5σ or greater. The dimmest source among this sub-sample had $f_X = 5.6 \times 10^{-12}\,\mathrm{ergs\,cm^{-2}\,s^{-1}}$, and the brightest had $f_X = 3.2 \times 10^{-10}\,\mathrm{ergs\,cm^{-2}\,s^{-1}}$. We derived a ML probability distribution, which can be approximated by a Gaussian, with our best fit parameters of $\alpha = 1.66 \pm 0.11$. A normalization of $K = 0.44\,\mathrm{sr}^{-1}\,(10^{-10}\,\mathrm{ergs\,cm^{-2}\,s^{-1}})^{\alpha}$ was then obtained by performing a least-squares fit, with the slope fixed to the ML value. The uncertainties in the final log N - log S primarily manifest in the normalization and it should not affect the slope significantly. Furthermore, the uncertainty in the detection limit will affect mainly the low flux end of the Log(N) – Log(S) distribution. The high flux end is less sensitive to scatter, since it is based on a larger sky area. To make a more quantitative assessment, we have recomputed the ML Log(N) – Log(S) calculation for scenarios in which the exposure time – flux limit curve shifted in amplitude and pivoted about the 700 ks point where we have the highest density of measurements. For those scenarios, we found that the inferred Log(N) – Log(S) slope varied by less than about 5%, which is contained within the range of our quoted 1-sigma uncertainty. The amplitude varied by as much as 7% in the extreme case, but for the pivoted cases, by only a few percent. We thus conclude that the maximum uncertainty resulting from possible systematics in our ef-

fective area correction is bounded by about 5% in slope and 7% in amplitude.

4. THE LOCAL LUMINOSITY FUNCTION OF AGN AT 20 – 40 KEV

The complete sample of *INTEGRAL* AGN with a detection significance $\geq 5\sigma$ also allows us to derive the density of these objects in the local Universe as a function of their luminosity. In order to derive the density of objects above a given luminosity, one has to determine for each source in a complete sample the space volume in which this source could have been found considering both the flux limit of each survey field and the flux of the object. We have again used the correlation between exposure time and flux limit as discussed in the previous section in order to assign a 5σ flux limit to each survey field. Then the maximum redshift z_{max} at which an object with luminosity L_X would have been detectable in each sky element was used to compute the total accessible volume

$$V_a = \sum_{i=1}^{N} \frac{\Omega_i}{4\pi} V_i[z_{max,i}(L_X)] \qquad (1)$$

with N being the number of sky elements in which the object would have been detectable and Ω_i the solid angle covered by sky element i, and V_i the enclosed volume based on the maximum redshift at which the object could have been detected in this sky element. Figure 2 shows the luminosity function in differential form. Blazars have been excluded because their emission is not isotropic. The redshifts in the sample range from $z = 0.001$ to $z = 0.129$ with an average redshift of $\bar{z} = 0.022$. Thus the luminosity function is truly a local one. The data points are independent of each other. In case one of the luminosity bins would suffer from incompleteness compared to the other bins, this would result in a break or dip in the differential luminosity function. The errors are based on the number of objects contributing to each value. The differential XLF shows a turnover around $L_X = (5-10) \times 10^{43}\,\mathrm{ergs\,s^{-1}}$.

Because our study is based solely on low redshift objects, we are not able to constrain models involving evolution with redshift. Nevertheless we can compare the XLF presented here with model predictions from previous investigations. XLFs are often fit by a smoothly connected two power-law function of the form [19]

$$\frac{d\phi(L_X, z=0)}{d\log L_X} = A \left[\left(\frac{L_X}{L_*} \right)^{\gamma_1} + \left(\frac{L_X}{L_*} \right)^{\gamma_2} \right]^{-1} \qquad (2)$$

We fit this function using a least-squares method. The best fit values we obtained are $A = 0.7^{+1.5}_{-0.5} \times 10^{-5}\,h_{70}^3\,\mathrm{Mpc^{-3}}$, $\gamma_1 = 0.80 \pm 0.15$, $\gamma_2 = 2.11 \pm 0.22$, and $\log L_* = 43.38 \pm 0.35$ with L_* in units of $h_{70}^{-2}\,\mathrm{ergs\,s^{-1}}$. The 1σ errors have been determined by applying a Monte Carlo simulation which simultaneously takes into account the flux errors on the individual sources, the error induced by deriving an average luminosity per bin, and the statistical error of the density based on the number of objects contributing to the density value. Each simulated data set included 9 luminosity values with a density value for each of them. These values where then fit by the smoothly connected two power-law function as described above. The scatter in the resulting parameters gave the error estimates as shown above.

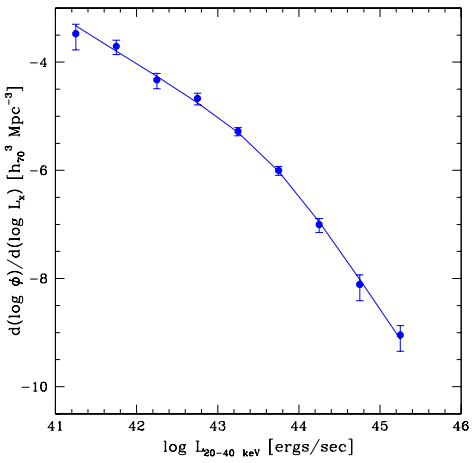

Figure 2. Differential luminosity function of AGN with $\Delta \log L_X = 0.5$ binning. The line shows a fit to a smoothly connected two power-law function with a turnover luminosity at $L_* = 2.4 \times 10^{43}\,\mathrm{ergs\,s^{-1}}$. Blazars have been excluded. The density ϕ describes the number of objects per Mpc^3 in a given luminosity interval.

The parameter values describing the differential luminosity function are consistent with values derived from the $2-10\,\mathrm{keV}$ XLF of AGN as shown by e.g. Ueda et al. (2003), La Franca et al. (2005), and Shinozaki et al. (2006). For example the work by Ueda et al. (2003) reveals for a pure density evolution model the same values (within the error bars) for γ_1 and γ_2, but a higher $\log L_* = 44.11 \pm 0.23$. The higher value can be easily explained by the different energy bands applied. A single power law with photon index of $\Gamma = 2$ in the range $2-40\,\mathrm{keV}$ would lead to $L_{(2-10\,\mathrm{keV})}/L_{(20-40\,\mathrm{keV})} = 2.3$, assuming no intrinsic absorption. This has, of course, no implications for the XLF at higher redshifts. The values are also consistent with the luminosity function for AGN in the $3-20\,\mathrm{keV}$ band as derived by Sazonov & Revnivtsev (2004) from the *RXTE* all-sky survey.

Information about intrinsic absorption is available for 32 of the 38 objects (89%) from soft X-ray observations. This enables us to derive the luminosity function for absorbed ($N_H \geq 10^{22}\,\mathrm{cm^{-2}}$) and unabsorbed sources, as shown in Figure 3. The absorbed sources have a higher density than the unabsorbed sources at low luminosities, while this trend is inverted at high luminosities. The lu-

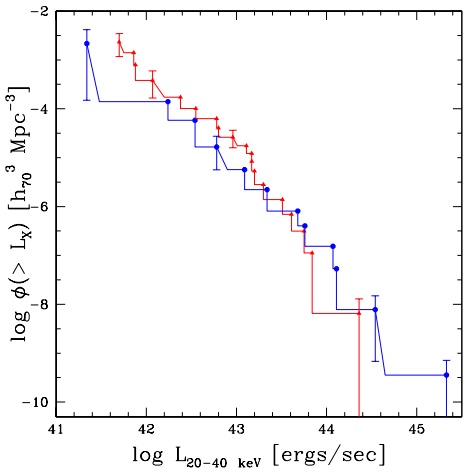

Figure 3. Cumulative AGN luminosity function for 19 absorbed ($N_H \geq 10^{22}\,\mathrm{cm}^{-2}$; triangles) and 12 unabsorbed sources (octagons). As an example some error bars indicating the Poissonian error are shown.

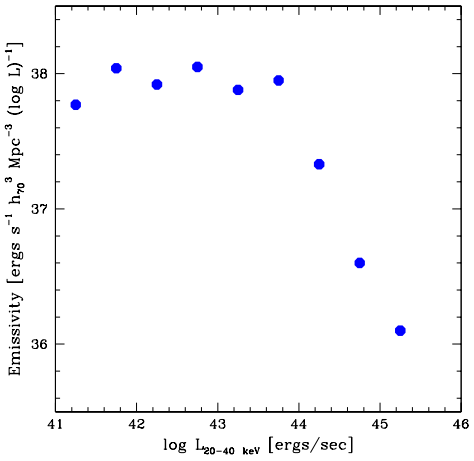

Figure 4. Emissivity of INTEGRAL AGN per unit volume and logarithmic luminosity bin. The objects with $L_X > 10^{44}\,\mathrm{ergs\,s}^{-1}$ do not contribute significantly to the total X-ray emissivity $W_{20-40\,\mathrm{keV}}(> 10^{41}\,\mathrm{ergs\,s}^{-1}) = (2.8 \pm 0.8) \times 10^{38}\,\mathrm{ergs\,s}^{-1}\,\mathrm{h}_{70}^3\,\mathrm{Mpc}^{-3}$.

minosity where both AGN types have similar densities is about $L_{(20-40\,\mathrm{keV})} = 3 \times 10^{43}\,\mathrm{erg\,s}^{-1}$.

Based on the luminosity function, the contribution of the AGN to the total X-ray emissivity W can be estimated [25]. This can be done by simply multiplying the XLF by the luminosity in each bin and integrating over the range of luminosities ($10^{41}\,\mathrm{ergs\,s}^{-1} < L_{20-40\,\mathrm{keV}} < 10^{45.5}\,\mathrm{ergs\,s}^{-1}$). This results in $W_{20-40\,\mathrm{keV}}(> 10^{41}\,\mathrm{ergs\,s}^{-1}) = (2.8 \pm 0.8) \times 10^{38}\,\mathrm{ergs\,s}^{-1}\,\mathrm{h}_{70}^3\,\mathrm{Mpc}^{-3}$. Please note that absorption does not affect the luminosities in this energy range and therefore the values given here are intrinsic emissivities. Figure 4 shows the emissivity per unit volume in discrete luminosity bins. Apparently, the objects with $L_X > 10^{44}\,\mathrm{ergs\,s}^{-1}$ do not contribute significantly to the total emissivity in the $20 - 40\,\mathrm{keV}$ energy band.

5. DISCUSSION

A simple power-law model fitted to the number flux distribution (Fig. 1) has a slope of $\alpha = 1.66 \pm 0.11$. Even though the difference from the Eucledian value is not statistically significant, at a 1.5σ level, a deviation from this value could have two reasons. The difference might indicate that the area density at the low flux end of the distribution has been slightly overcorrected. One has to keep in mind that only a few sources derived from a small area of the sky are constraining the low flux end. Another reason for the difference could be that the distribution of AGN in the very local universe is not isotropic, caused e.g. by the local group and other clustering of galaxies. Krivonos et al. (2005) studied the extragalactic source counts as observed by *INTEGRAL* in the 20-50 keV energy band in the Coma region. Based on 12 source detections they determine a surface density of $(1.4 \pm 0.5) \times 10^{-2}\,\mathrm{deg}^{-2}$ above a threshold of $10^{-11}\,\mathrm{ergs\,cm}^{-2}\,\mathrm{s}^{-1}$ in the $20 - 50\,\mathrm{keV}$ energy band, where we get a consistent value of $(1.2 \pm 0.2) \times 10^{-2}\,\mathrm{deg}^{-2}$. Comparing the total flux of all the objects in the AGN sample ($f_{20-40\,\mathrm{keV}} = 2.6 \times 10^{-10}\,\mathrm{ergs\,cm}^{-2}\,\mathrm{s}^{-1}\,\mathrm{sr}^{-1}$) with the flux of the X-ray background as presented by Gruber et al. (1999) shows that the *INTEGRAL* AGN account only for about 1% of the expected value. This is expected when taking into account the high flux limit of our sample: La Franca et al. (2005) have shown that objects with $f_{2-10\,\mathrm{keV}} > 10^{-11}\,\mathrm{ergs\,cm}^{-2}\,\mathrm{s}^{-1}$ contribute less than 1% to the CXB in the $2 - 10\,\mathrm{keV}$ energy range. This flux limit extrapolates to the faintest flux in our sample of $f_{20-40\,\mathrm{keV}} = 5.6 \times 10^{-12}\,\mathrm{ergs\,cm}^{-2}\,\mathrm{s}^{-1}$ for a $\Gamma = 1.9$ power law spectrum.

We compared the unabsorbed emissivity per unit volume of our objects $W_{20-40\,\mathrm{keV}}(> 10^{41}\,\mathrm{ergs\,s}^{-1}) = 2.8 \times 10^{38}\,\mathrm{ergs\,s}^{-1}\,\mathrm{h}_{70}^3\,\mathrm{Mpc}^{-3}$ with that observed by *RXTE* in the 3–20 keV band. Assuming an average power law of $\Gamma = 2$, the extrapolated value is $W_{3-20\,\mathrm{keV}}(> 10^{41}\,\mathrm{ergs\,s}^{-1}) = (7.7 \pm 2.2) \times 10^{38}\,\mathrm{ergs\,s}^{-1}\,\mathrm{h}_{70}^3\,\mathrm{Mpc}^{-3}$, which is a factor of 2 larger than the value measured by *RXTE* [25] but consistent within the 1σ error. If we apply the conversion to the $2 - 10\,\mathrm{keV}$ energy band, we derive the intrinsic emissivity $W_{2-10\,\mathrm{keV}} = (6.4 \pm 1.8) \times 10^{38}\,\mathrm{ergs\,s}^{-1}\,\mathrm{Mpc}^{-3}$, consistent with the value derived from the *HEAO-1* measurements ($W = (5.9 \pm 1.2) \times 10^{38}\,\mathrm{ergs\,s}^{-1}\,\mathrm{Mpc}^{-3}$; Shinozaki et al. 2006). This showed that the local X-ray volume emissivity in the 2–10 keV band is consistent with the emissivity from AGN alone. It has to be pointed out that the value derived from our sample and the one based on *HEAO-1* data are higher than the one based on the *RXTE* All-Sky Survey ($W = (2.7 \pm 0.7) \times 10^{38}\,\mathrm{ergs\,s}^{-1}\,\mathrm{Mpc}^{-3}$; Sazonov & Revnivtsev 2004).

The luminosity function derived from the *INTEGRAL* $20-40\,\mathrm{keV}$ AGN sample appears to be consistent with the XLF in the $2-20\,\mathrm{keV}$ range. A turnover in the XLF at $\simeq 2.4\times10^{43}\,\mathrm{ergs\,s^{-1}}$ is observed (Fig. 2). Below this luminosity also the fraction of absorbed AGN starts to exceed that of the unabsorbed ones, although the effect is significant at only on a 1σ level (Fig. 3). Both effects have been seen also in the $2-10\,\mathrm{keV}$ [31, 17, 29] and in the $3-20\,\mathrm{keV}$ band [25]. This implies that we do detect a similar source population as at lower energies.

Even though it has to be taken into account that the low luminosity end of the XLF is based only on a small number of objects, below this luminosity the distribution between active and normal galaxies becomes blurred. Additionally objects like Ultra-luminous X-ray sources (ULX) and star-forming galaxies could provide the necessary emission. One interesting case in this category is the detection of NGC 4395 with a luminosity of $L_{(20-40\,\mathrm{keV})}=1.4\times10^{40}\,\mathrm{ergs\,s^{-1}}$, consistent with measurements by *XMM-Newton* which showed $L_{(2-10\,\mathrm{keV})}=1.5\times10^{40}\,\mathrm{ergs\,s^{-1}}$ [33]. The central engine of this galaxy has been classified as an "ultra-luminous" source, possibly associatied with an intermediate mass black hole with $M_{BH}=(4^{+6}_{-3}\times10^{4}\,\mathrm{M_\odot}$ [22]. In addition, NGC 4395 harbors a ULX with $L_{(2-10\,\mathrm{keV})}=10^{39}\,\mathrm{ergs\,s^{-1}}$ at a distance of $2.9\,\mathrm{kpc}$ from the center of the galaxy [8].

If a larger fraction of absorbed AGN is necessary to explain the cosmic X-ray background at $\sim 30\,\mathrm{keV}$ as indicated by *HEAO 1* A-4 measurements [13], the fraction of absorbed sources could be correlated with redshift. It has for example been proposed that there is an evolution of the population leading to a higher fraction of absorbed sources at higher redshifts. It should be noted however that this effect is not clearly detectable in the $2-10\,\mathrm{keV}$ range. The fraction of absorbed sources seems to depend on luminosity [31, 30], as is also seen in the $20-40\,\mathrm{keV}$ band (Fig. 3). But some studies come to the conclusion that there is no evolution of intrinsic N_H [31, 30], while others find the fraction of absorbed sources increasing with redshift [17]. La Franca et al. also find that a combination of effects (the fraction of absorbed AGN decreases with the intrinsic X-ray luminosity, and increases with the redshift) can be explained by a luminosity-dependent density evolution model. They further show that the luminosity function of AGN with low luminosities as those presented here peaks at $z\sim0.7$ while high luminosity AGN peak at $z\sim2$. Unified models also predict, depending on the applied model, a fraction of absorbed AGN of $0.6-0.7$ compared to the total population for high-flux low-redshift objects [30]. Worsley et al. (2005) examined *Chandra* and *XMM-Newton* deep fields and come to the conclusion that the missing CXB component is formed by highly obscured AGN at redshifts $\sim0.5-1.5$ with column densities of the order of $f_X=10^{23}-10^{24}\,\mathrm{cm^{-2}}$. Evidence for this scenario is also found in a study of *Chandra* and *Spitzer* data [24]. Combining multiwavelength data, this work estimates a surface density of $25\,\mathrm{AGN\,deg^{-2}}$ in the infrared in the $0.6\,\mathrm{deg^2}$ *Chandra*/SWIRE field, and only 33% of them are detected in the X-rays down to $f_{0.3-8\,\mathrm{keV}}=10^{-15}\,\mathrm{ergs\,cm^{-2}\,s^{-1}}$. The work also indicates a higher abundance of luminous and Compton-thick AGN at higher redshifts ($z\gg0.5$). This source population would be missed by the study presented here, because of the low redshifts ($\bar{z}=0.022$) of the *INTEGRAL* AGN.

Several studies [31, 30] propose that the absorbed AGN needed to explain the CXB should be Compton thick, and therefore would have been missed at $2-10\,\mathrm{keV}$. This argument does not hold for the *INTEGRAL* observations, where the impact of absorption is much less severe than at lower energies. The effect on the measured flux of a source with photon index $\Gamma=2$ for Compton thick absorption ($N_H=10^{24}\,\mathrm{cm^{-2}}$) is only a 5% decrease in flux (40% for $N_H=10^{25}\,\mathrm{cm^{-2}}$). It is therefore unlikely that many Compton-thick objects have been missed by the *INTEGRAL* studies performed to date. One possibility would be, that they are among the newly discovered sources found by *INTEGRAL*. The fraction of unidentified objects among the *INTEGRAL* discovered sources is approximately 50%. Eight such sources without cross-identification have a significance above 5σ in the data set discussed here. Thus, if they are ultimately identified as AGN, they would have to be considered in this study. It should be pointed out though, that most of the sources discovered by *INTEGRAL* are located close to the Galactic plane and are more likely to belong to the Galaxy: the Second IBIS/ISGRI Soft Gamma-Ray Survey Catalog [5] lists 55 new sources detected by *INTEGRAL*, of which 93% are located within $-10^\circ<b<+10^\circ$. Among these 55 sources, 3 are listed as extragalactic sources, 18 are of Galactic origin, and 29 have not been identified yet.

In addition, those objects that have been classified as AGN based on soft X-ray and/or optical follow-up studies, are no more likely to be Compton-thick objects than the overall AGN population studied here. Only four AGN (NGC 1068, NGC 4945, MRK 3, Circinus galaxy) detected by *INTEGRAL* have been proven to be Compton thick objects so far, and none of them showed absorbtion of $N_H>5\times10^{24}\,\mathrm{cm^{-2}}$. In order to clarify this point, observations at soft X-rays of those objects without information about intrinsic absorption are required for all *INTEGRAL* detected AGN. At present 23 % of the *INTEGRAL* AGN are missing absorption information. A first indication of what the absorption in these sources might be, can be derived from comparison of the *INTEGRAL* fluxes with *ROSAT* All-Sky Survey (RASS) Faint Source Catalogue data [34]. In order to do so we assumed a simple power law with photon index $\Gamma=2.0$ between the *ROSAT* $0.1-2.4\,\mathrm{keV}$ band and the *INTEGRAL* $20-40\,\mathrm{keV}$ range and fit the absorption. In the six cases where no detection was achieved in the RASS, an upper limit of $f_{(0.1-2.4\,\mathrm{keV})}\leq10^{-13}\,\mathrm{ergs\,cm^{-2}\,s^{-1}}$ has been assumed, resulting in a lower limit for the absorption $N_H>(5-11)\times10^{22}\,\mathrm{cm^{-2}}$. In Fig. 5 we show the distribution of intrinsic absorption. It has to be pointed out that the estimated values can only give an idea about the distribution of intrinsic absorption and should not be taken literally, as the spectral slope between the measure-

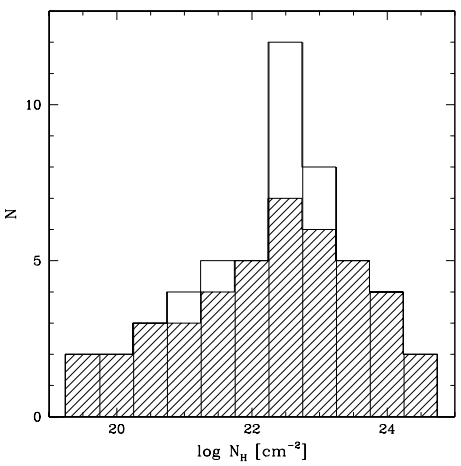

Figure 5. Distribution of intrinsic absorption for all INTEGRAL AGN (blazars excluded), as measured in the soft X-rays. The shaded area shows the reliable measurements, the other values are based on comparison of ROSAT All-Sky Survey and INTEGRAL data. Lower limits on absorption have been excluded.

ments is unknown and the observations are not simultaneous. Nevertheless apparently none of the RASS detections and non-detections requires an intrinsic absorption of $N_H > 2 \times 10^{23}\,\mathrm{cm}^{-2}$. Therefore it appears unlikely that a significant fraction of *INTEGRAL* AGN will show an intrinsic absorption $N_H > 10^{24}\,\mathrm{cm}^{-2}$. However, if we assume that the RASS non-detections are all Compton thick AGN, the fraction of this class of sources rises from 6% to 16% when considering all 63 non-blazar AGN seen by *INTEGRAL*, and from 8% to 13% for the complete sample with 38 objects. This is in good agreement with the fraction of 11% of Compton thick AGN as seen in the *Swift*/BAT survey [20]. The picture is less clear when referring to the optical classification. Here the *INTEGRAL* survey finds 12 Seyfert 1 (33%), 14 Seyfert 2, and 10 intermediate Seyfert 1.5 in the complete sample, while the *Swift*/BAT survey contains only 20% of type 1 Seyfert galaxies. It should be pointed out though that the classification based on intrinsic absorption gives a more objective criterion in order to define AGN subclasses than the optical classification with its many subtypes. The finding of the BAT survey that virtually all sources with $\log L_X < 43.5$ are absorbed, cannot be confirmed by our study, in which we detect a fraction of 33% of sources with $N_H < 10^{22}\,\mathrm{cm}^{-2}$ among the sources below this luminosity. This also reflected in the observation that although the absorbed sources become more dominant below this luminosity, the trend is not overwhelmingly strong (Fig. 3).

Most investigations to date have been focused on the X-rays below 20 keV, and *INTEGRAL* can add substantial information to the nature of bright AGN in the local Universe. Considering the expected composition of the hard X-ray background, it does not currently appear that the population detected by *INTEGRAL* can explain the peak at 30 keV, as Compton thick AGN are apparently less abundant than expected [30]. But this picture might change if we assume all *INTEGRAL* AGN lacking soft X-ray data and without counter parts in the RASS to be Compton thick. In addition the sample presented here might be still too small to constrain the fraction of obscured sources, and the missing Compton thick AGN could be detectable when studying sources with $f_{(20-40\,\mathrm{keV})} < 10^{-11}\,\mathrm{ergs\,cm^{-2}\,s^{-1}}$.

6. CONCLUSIONS

The extragalactic sample derived from the *INTEGRAL* public data archive comprises 63 low redshift Seyfert galaxies ($\langle z \rangle = 0.022 \pm 0.003$) and 8 blazars in the hard X-ray domain. Two galaxy clusters are also detected, but no star-burst galaxy has been as yet. This *INTEGRAL* AGN sample is the basis for the first luminosity function above 20 keV. 38 of the Seyfert galaxies form a complete sample with significance limit of 5σ.

The number flux distribution is approximated by a power-law with a slope of $\alpha = 1.66 \pm 0.11$. Because of the high flux limit of our sample the objects account in total for less than 1% of the $20 - 40\,\mathrm{keV}$ cosmic X-ray background. The emissivity of all AGN per unit volume $W_{20-40\,\mathrm{keV}}(> 10^{41}\,\mathrm{ergs\,s^{-1}}) = 2.8 \times 10^{38}\,\mathrm{ergs\,s^{-1}\,h_{70}^{3}\,Mpc^{-3}}$ appears to be consistent with the background estimates in the 2–10 keV energy band based on the cross-correlation of the *HEAO 1*-A2 map with *IRAS* galaxies [23].

The luminosity function in the $20 - 40\,\mathrm{keV}$ energy range is consistent with that measured in the $2 - 20\,\mathrm{keV}$ band. Below the turnover luminosity of $L_* = 2.4 \times 10^{43}\,\mathrm{ergs\,s^{-1}}$ the absorbed AGN become dominant over the unabsorbed ones. Similar results have been derived by Sazonov et al. (2007) using a larger *INTEGRAL* data set and a slightly different energy band ($17 - 60\,\mathrm{keV}$), including 91 AGN above the 5σ significance limit.

The fraction of Compton thick AGN with known intrinsic absorption is found to be small (8%) in our AGN sample. For the sources without reliable absorption information we derived an estimate from the comparison with *ROSAT* All-Sky Survey data and find that the data do not require additional Compton thick objects within the sample presented here. It has to be pointed out though, that the sources without RASS counterpart could be Compton thick which would increase the ratio of this source type to 13% in the complete sample. Evolution of the source population can play a major role in the sense that the fraction of absorbed sources among AGN might be correlated with redshift, as proposed for example by Worsley et al. (2005).

Over the life time of the *INTEGRAL* mission we expect to detect of the order of 250 AGN. Combining these data with the studies based on *Swift*/BAT, operating in a similar energy band as IBIS/ISGRI, will further constrain the

hard X-ray luminosity function of AGN. But we will still be limited to the relatively high flux end of the distribution. Because of this *INTEGRAL* and *Swift*/BAT will most likely not be able to test evolutionary scenarios of AGN and thus will be inadequate to explain the cosmic X-ray background at $E > 20\,\mathrm{keV}$. Future missions with larger collecting areas and/or focusing optics will be required to answer the question of what dominates the Universe in the hard X-rays.

ACKNOWLEDGMENTS

VB would like to thank Olaf Wucknitz for providing software to handle the $\Lambda_0 > 0$ cosmology. This research has made use of the NASA/IPAC Extragalactic Database (NED) which is operated by the Jet Propulsion Laboratory, of data obtained from the High Energy Astrophysics Science Archive Research Center (HEASARC), provided by NASA's Goddard Space Flight Center, and of the SIMBAD Astronomical Database which is operated by the Centre de Données astronomiques de Strasbourg. This research has also made use of the Tartarus (Version 3.1) database, created by Paul O'Neill and Kirpal Nandra at Imperial College London, and Jane Turner at NASA/GSFC. Tartarus is supported by funding from PPARC, and NASA grants NAG5-7385 and NAG5-7067.

REFERENCES

[1] Avni Y., Bahcall J. N. 1980, ApJ, 235, 694

[2] Beckmann V., Gehrels N., Shrader C. R., & Soldi S. 2006a, ApJ, 638, 642

[3] Beckmann V., Soldi S., Shrader C. R., & Gehrels N. 2006b, proc. of "The X-ray Universe 2005", San Lorenzo de El Escorial (Madrid, Spain), 26-30 September 2005, ESA-SP 604, astro-ph/0510833

[4] Beckmann V., Soldi S., Shrader C. R., Gehrels N., & Produit N., 2006c, ApJ, 652, 126

[5] Bird A., et al. 2006, ApJ, 636, 765

[6] Brandt W. N., et al. 2001, AJ, 122, 2810

[7] Brandt W. N., Hasinger G. 2005, ARA&A, 43

[8] Colbert E. J. M., Ptak A. F. 2002, ApJSS, 143, 25

[9] Comastri A., Fiore F., Vignali C., et al. 2001, MNRAS, 327, 781

[10] Courvoisier T.J.-L., Walter R., Beckmann V., et al. 2003, A&A, 411, L53

[11] Gehrels N., et al. 2005, ApJ, 611, 1005

[12] Giacconi R., Gursky H., Paolini R., & Rossi B. 1962, Phys. Rev. Lett., 9, 439

[13] Gruber D. E., Matteson J. L., Peterson L. E., & Jung G. V. 1999, ApJ, 520, 124

[14] Hasinger G., Burg R., Giacconi R., et al. 1998, A&A, 329, 482

[15] Hasinger G. 2004, Nucl. Phys. B (Proc. Suppl.), 132, 86

[16] Krivonos R., Vikhlinin A., Churazov E., et al. 2005, ApJ, 625, 89

[17] La Franca F., et al. 2005, ApJ, 635, 864

[18] Lebrun F., et al. 2003, A&A, 411, L141

[19] Maccacaro T., Della Ceca R., Gioia I. M., et al. 1991, 374, 117

[20] Markwardt C. B., Tueller J., Skinner G. K., et al. 2005, ApJ, 633, L77

[21] Marshall F. E., et al. 1980, ApJ, 235, 4

[22] McHardy I. M. M., Gunn K. F., Uttley P., & Goad M. R. 2005, MNRAS, 359, 1469

[23] Miyaji T., Lahav O., Jahoda K., & Boldt E. 1994, ApJ, 434, 424

[24] Polletta M., et al. 2006, ApJ, 642, 673

[25] Sazonov S. Y., Revnivtsev M. G. 2004, A&A, 423, 469

[26] Sazonov S. Y., Revnivtsev M., Krivonos R., Churazov E., & Sunyaev R., 2007, A&A, 462, 57

[27] Schmidt M., et al. 1998, A&A, 329, 495

[28] Setti G., Woltjer L. 1989, A&A, 224, L21

[29] Shinozaki K., Miyaji T., Ishisaki Y., et al. 2006, AJ, 131, 2843

[30] Treister E., Urry C. M. 2005, ApJ, 630, 115

[31] Ueda Y., Akiyama M., Ohta K., & Miyaji T. 2003, ApJ, 598, 886

[32] Ueda Y., Ishisaki Y., Takahashi T., et al. 2001, ApJS, 133, 1

[33] Vaughan S., Iwasawa K., Fabian A. C., & Hayashida K. 2004, MNRAS, 356, 524

[34] Voges W., et al. 2000, IAUC, 7432, 3

[35] Worsley M. A., et al. 2005, MNRAS, 357, 1281